Weather Radar Network Benefit Model for Flash Flood Casualty Reduction

JOHN Y. N. CHO AND JAMES M. KURDZO

Lincoln Laboratory, Massachusetts Institute of Technology, Lexington, Massachusetts

(Manuscript received 15 July 2019, in final form 12 February 2020)

ABSTRACT

A monetized flash flood casualty reduction benefit model is constructed for application to meteorological radar networks. Geospatial regression analyses show that better radar coverage of the causative rainfall improves flash flood warning performance. Enhanced flash flood warning performance is shown to decrease casualty rates. Consequently, these two effects in combination allow a model to be formed that links radar coverage to flash flood casualty rates. When this model is applied to the present-day contiguous U.S. weather radar network, results yield a flash flood–based benefit of $316 million (M) yr^{-1}. The remaining benefit pools are more modest ($13 M yr^{-1} for coverage improvement and $69 M yr^{-1} maximum for all areas of radar quantitative precipitation estimation improvements), indicative of the existing weather radar network's effectiveness in supporting the flash flood warning decision process.

1. Introduction

Weather radars are generally acknowledged to be a valuable asset to society (e.g., Saunders et al. 2018). They provide observational data that improve weather forecasts and present essential situational awareness to many users. Radars, however, are expensive to acquire, operate, and maintain. In planning for future sensor networks, monetization of their benefits is needed to assess the trade-off between more expensive options (higher performance and/or coverage) and benefits (people's lives and time saved).

Although meteorological radar observations help to improve weather forecast model performance through data assimilation (e.g., Stensrud et al. 2009), their most direct impacts are made through the detailed and continuously updated depiction of precipitating weather for real-time decision-making. Sometimes these decisions are life-or-death matters. In the last 30 years (1989–2018), the top three weather-related fatality causes in the United States were excessive heat, floods, and tornadoes (NOAA 2019). The National Weather Service (NWS) issues warnings for these hazards, and weather radar data play an absolutely crucial role for the latter two (Polger et al. 1994). Thus, we focused on tornadoes and floods in quantifying the benefits that meteorological radars provide to society. A benefit model for tornadoes was published previously (Cho and Kurdzo 2019a,b, hereinafter CK19a,b). In this paper, we move on to a benefit model for heavy-rain-induced flash floods.

For this study, we hypothesized that better weather radar coverage improves flash flood warning performance, which, in turn, reduces casualties. The second half of this causality chain is intuitive. Flash flood warnings can provide the impacted populace time to take appropriate action to help prevent loss of life and potentially reduce property damage (e.g., Sene 2013). Empirical evidence exists that such warnings do decrease flash flood fatalities (e.g., DeKay and McClelland 1993). The first half of the proposed causality chain, however, requires more explanation on how flash flood warning decisions are made.

In the United States, operational flash flood warning decisions rely primarily on the concept of flash flood guidance (FFG; Ostrowski et al. 2003). Based on basin hydrological models with soil moisture and streamflow as initial conditions, FFG outputs rainfall accumulation needed in 1-, 3-, 6-, or 12-h periods to cause flash flood conditions on a typical small stream or urban area in the region of interest. There are different types of FFG models used at different weather forecast offices (WFOs)—lumped FFG, gridded FFG, distributed FFG, and flash flood potential index. However, regardless of type, the basic idea is that the forecaster looks for accumulated quantitative precipitation estimation (QPE)

Corresponding author: John Y. N. Cho, jync@ll.mit.edu

DOI: 10.1175/JAMC-D-19-0176.1

© 2020 American Meteorological Society. For information regarding reuse of this content and general copyright information, consult the AMS Copyright Policy (www.ametsoc.org/PUBSReuseLicenses).

Brought to you by NOAA Central Library | Unauthenticated | Downloaded 01/16/24 09:14 PM UTC

to exceed the FFG rain accumulation threshold in a given catchment basin when issuing a flash flood warning; decision support tools such as the flash flood monitoring and prediction system aid the forecaster in this process (Clark et al. 2014).

By definition, flash floods occur within 6 h of the causative event (NWS 2019). Thus, when the cause is heavy rain, in order for the WFO to issue a timely flash flood warning, forecasters mostly utilize multisensor precipitation estimator (MPE) products for comparison with FFG thresholds. (Waiting for flow-level measurements from stream gauges delays the decision, and, in any case, many potential flash flood areas are in ungauged headwaters.) MPE ingests radar, rain gauge, and geostationary satellite data; rain gauge data are used to help correct biases in the radar and satellite estimates. The dominant MPE contributor is radar QPE, while satellite QPE is mainly used to fill gaps in radar coverage (Kitzmiller et al. 2013). Also, with finer-spatial-resolution hydrological models becoming feasible for operational use, the value of highly resolved rainfall estimates from radars is expected to rise in the future (Gourley et al. 2014). Forecasters have started to consult short-term rainfall nowcasts as well (Ahnert et al. 2012).

The flash flood warning decision process, therefore, depends on the accuracy of the FFG and MPE products. FFG threshold errors are dependent on FFG type and are specific to each catchment basin. There are various sources of MPE errors, including those for radar QPE such as choice of algorithm, radar calibration, and rain gauge density (e.g., Cecinati et al. 2017). The situation is further complicated by the fact that the WFOs do not utilize a uniform set of data products and decision support tools. To analyze the impacts of input data errors on flash flood warning performance would require an in-depth case study at a particular WFO using a detailed hydrological model of a catchment basin—this is not conducive to a national-scale statistical analysis.

In this study, we took a simple approach. Since poor radar coverage is a significant source of radar QPE error (Rogalus and Ogden 2013; Kurdzo et al. 2018), we hypothesized that flash flood warning performance would depend on radar coverage, even without taking into account the other error sources in the warning decision process—this is proved true in sections 2d and 2e. By linking radar coverage directly to warning performance, we bypassed the very complex problem of characterizing MPE and FFG product errors, considerably simplifying the analysis. We believe a clear statistical signal was extractable due to the large number of cases nationwide used in the analysis.

To summarize briefly, we propose an original geospatial model for monetizing flash flood casualty reduction benefits of a meteorological radar network. This analysis, along with the earlier tornado benefit effort (CK19a,b), was conducted for the National Oceanic and Atmospheric Administration (NOAA) as part of a larger program that is studying future radar systems beyond the Weather Surveillance Radar-1988 Doppler (WSR-88D). Benefits must be weighed carefully against costs in considering advanced technologies such as active phased array radars (Weber et al. 2007; Zrnić et al. 2007) and/or a denser network of smaller radars (McLaughlin et al. 2009).

In addressing the complex nature of the problem, we employed only the bare essentials in objectively modeling the radar effects. In contrast to detailed hydrological simulation or survey-based case studies, we relied on the power of large datasets to yield statistically meaningful results with simple models. We made conservative choices when there was uncertainty. Statistically insignificant variables were disregarded. Our geographic scope was limited to the contiguous United States (CONUS), as that is where most of the relevant data were available and wide variation in radar coverage exists.

2. Model development

Following the successful radar network benefit modeling approach of CK19a,b for tornadoes, we sought to establish statistical relationships using historical flash flood data 1) between radar coverage metrics and flash flood warning performance and 2) between flash flood warning performance and casualty rate. With these two links established, the flash flood casualty rate could be computed geospatially for any given weather radar network. With casualty monetized, the difference between a baseline case (e.g., the current WSR-88D network) and a hypothetical radar network would yield the benefit (or loss). The methods used throughout follow closely those used by CK19a,b.

To provide a visual aid for understanding both the model development process and the model usage, Fig. 1 gives high-level block diagram views of these procedures. The reader is encouraged to refer back to this figure while reading the detailed explanations in the following sections.

a. Analysis data source and time period

We needed to use as many data as possible to achieve statistically significant results. At the same time, however, we had to maintain uniform conditions for unbiased regression results. Our primary source was the U.S. Flash Flood Observation Database (Gourley et al. 2013) compiled by the Flooded Locations and Simulated Hydrographs (FLASH) project (Gourley et al. 2017). Although the earliest-processed NWS storm reports in

Brought to you by NOAA Central Library | Unauthenticated | Downloaded 01/16/24 09:14 PM UTC

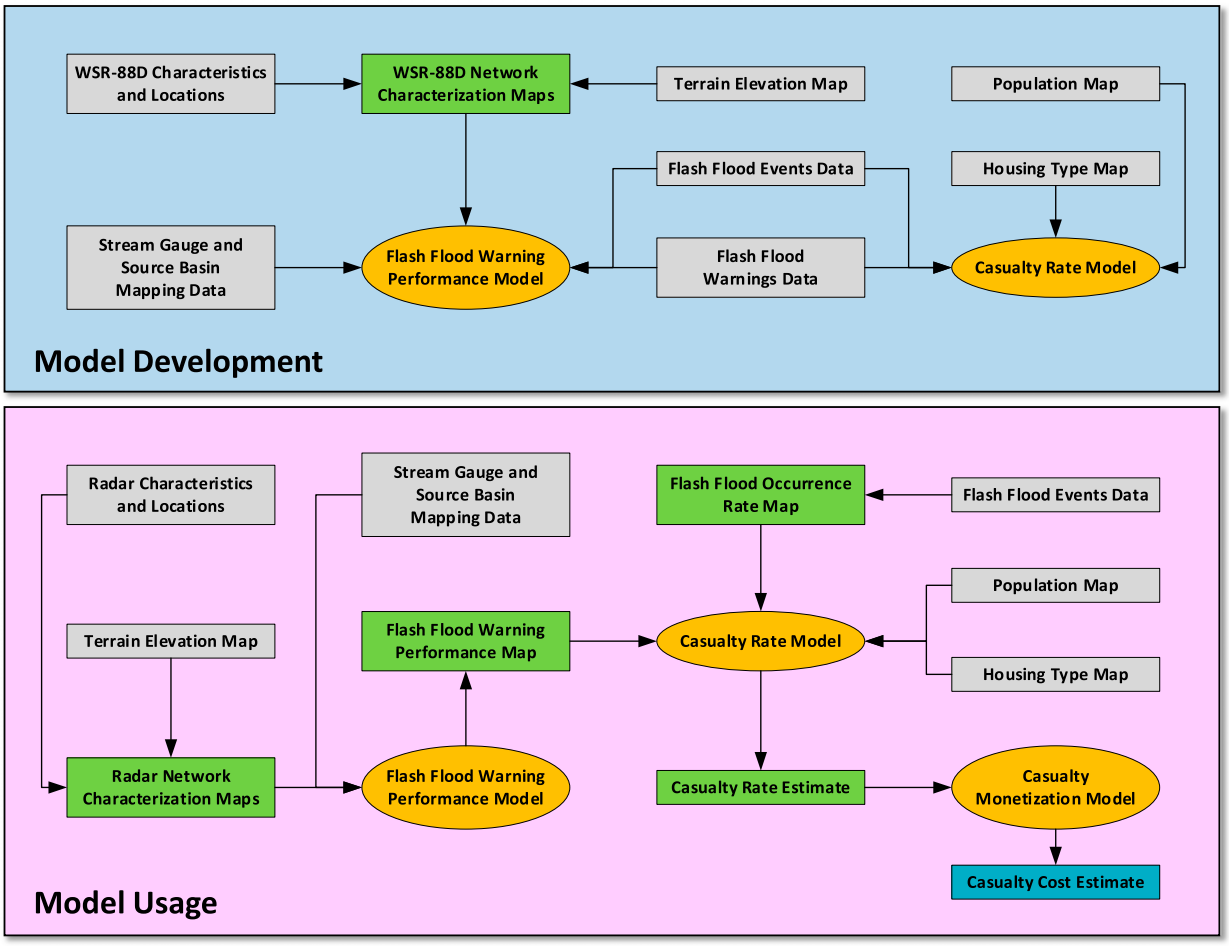

FIG. 1. Development and usage block diagrams of the radar network flash flood casualty cost model. Input data are indicated by gray rectangles, intermediate data products are shown by green rectangles, and final monetized cost output is given by a blue rectangle. Computational model units are shown as orange ovals.

the FLASH database are from 2006, the official transition from county-based flash flood reporting (a single point indicating an event somewhere in the county) to polygon-based reporting did not occur until 1 October 2007. Thus, we limited our analysis period to begin on this transition date (the transition from county-based to storm-based warnings also took place on the same day). Furthermore, because the FLASH storm report database only extended to July 2013, we supplemented those data with storm reports pulled from NOAA's National Centers for Environmental Information (https://www.ncdc.noaa.gov/stormevents/) up to 31 December 2018, which we then processed to match the content and format of the FLASH data. This yielded about 12 years of flash flood data to analyze. Only reports with an associated cause of "heavy rain" were retained.

Storm warning data for the matching period were obtained from the Iowa Environmental Mesonet NWS Watch/Warnings archive (https://mesonet.agron.iastate.edu/request/gis/watchwarn.phtml). If any part of the flash flood polygon was inside the warning polygon and if any segment of the flash flood time span overlapped the warning valid interval, then the warning was considered a hit; otherwise, it was labeled a false alarm. The lead time for a hit was computed as the beginning time of the flash flood minus the initial warning issuance time. For the remainder of the paper, we will refer to the fraction of flash floods with warning interchangeably with probability of detection (POD) for brevity.

b. *Radar coverage metrics*

The radar observational characteristics important for QPE accuracy are vertical coverage, horizontal resolution, and availability of dual-polarization products (Kurdzo et al. 2019, manuscript submitted to *J. Appl. Meteor. Climatol.*). The data update rate might

Brought to you by NOAA Central Library | Unauthenticated | Downloaded 01/16/24 09:14 PM UTC

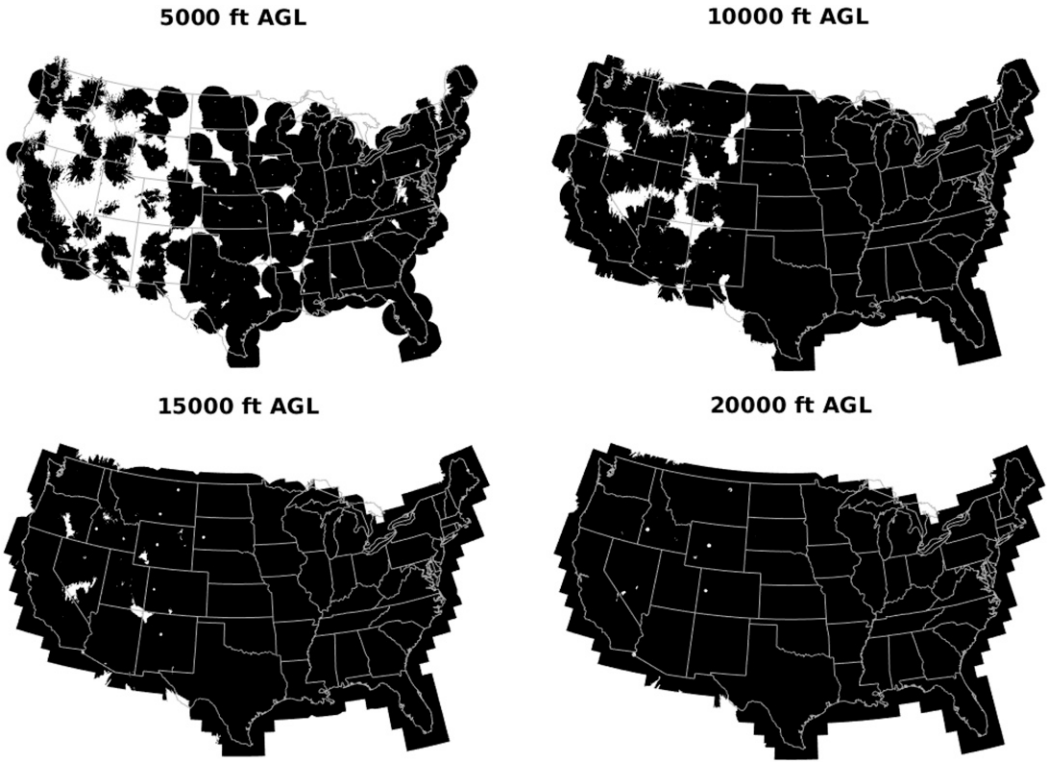

FIG. 2. WSR-88D coverage at the indicated height slices.

also have an impact on flash flood warning performance. An ongoing study aims to answer this question, and early results show that QPE from faster radar scans can improve agreement between measured and simulated stream gauge levels during flash floods (Wen et al. 2018).

With vertical coverage, the most crucial aspect is the radar antenna beam's minimum height above ground level (AGL), since the aim of QPE is to match the rainfall measurement at the surface. However, information aloft is also useful to forecasters for determining location of the radar bright band (Austin and Bemis 1950), regions of mixed-phase precipitation (Balakrishnan and Zrnić 1990), and for ingest to QPE correction algorithms such as vertical profiles of reflectivity (VPR; Kirstetter et al. 2010). Additionally, future uses such as quasi-vertical profiles (QVP; Ryzhkov et al. 2016) may be of use to forecasters for determining rainfall rates. Thus, we decided to employ the same coverage metric, fraction of vertical volume observed (FVO) between 0 and 20 kft AGL (1 kft = 304.8 m), as we did for the CK19a,b tornado study. The rationale for picking 20 kft as the FVO ceiling is that the current WSR-88D network (on which we base the statistical analysis) has essentially perfect coverage above 20 kft (Fig. 2); therefore, no information content is added by moving the ceiling higher, whereas moving it lower progressively eliminates actual deficiencies in coverage from consideration. FVO includes the effects of Earth's curvature, terrain blockage, and the radar's overhead "cone of silence" resulting from its limited elevation scanning angle, so it is a convenient and effective metric.

Details of the beam blockage calculations are given by Cho (2015). The minimum and maximum elevation coverage angles were assumed to be 0° and 20°, roughly corresponding to the bottom and top sides of the main antenna lobe at the WSR-88D scan angle limits of 0.5° and 19.5°. These limits are approximations, because the maximum elevation angles vary for different volume coverage patterns (VCPs) and the minimum angle has recently been lowered slightly at a few high-altitude sites (Steadman and Brown 2007).

Cross-radial horizontal resolution (CHR), which is approximately range times azimuthal angular resolution, is also relevant. (Along-range horizontal resolution is constant everywhere for monostatic radars, so it is not of value here.) Azimuthal angular resolution is dependent on dwell length and antenna beamwidth (Zrnić and Doviak 1976). The WSR-88D beamwidth is just under 1°. Presently, it has a "superresolution" mode that outputs data every 0.5°; however, the effective angular resolution is about 1° based on the antenna beamwidth

Brought to you by NOAA Central Library | Unauthenticated | Downloaded 01/16/24 09:14 PM UTC

and time series data window (Torres and Curtis 2006). Taking all this into account, we took the angular resolution to be 1° for the analysis period. Consequently, for the current WSR-88D, the resulting CHR is functionally the same as the distance from the radar. CHR could become a more meaningful performance metric, since future radar networks may have varying angular resolutions—for example, with a mix of powerful narrow-beam radars augmented by gap-filling broad-beam systems (Chandrasekar et al. 2012), or with the angle-dependent resolution of fixed planar phased arrays (Weber et al. 2017).

During the analysis period (October 2007 to December 2018), the WSR-88D CONUS network underwent two relevant changes. First, a new radar was added at Langley Hill, Washington, in September 2011. Second, the network was upgraded from single polarization to dual polarization. To address the first change, we produced two sets of FVO and CHR maps corresponding to before and after the Langley Hill deployment. For the second network change, we conducted our analysis over the entire database time span as well as the single-polarization period and the post-dual-polarization upgrade period. To ensure that there would be no cross contamination between the two polarization eras, the end of the single-polarization period was marked by the first operational CONUS deployment of dual polarization (8 March 2011), and the start of the dual-polarization period was marked by the completion of CONUS deployment (16 May 2013).

Although we included terminal Doppler weather radars (TDWRs) in our earlier analysis for tornadoes, because we determined that forecasters utilize TDWR data for tornado warning decisions, we did not include them for flash floods, since TDWRs are not used for QPE purposes.

c. *Mapping flash flood event to corresponding basin*

Flooding location is different from the place where the causative rain falls. To study the relationship between the quality of radar coverage (which affects QPE accuracy) and flash flood warning performance, we had to match each flood event to the appropriate upstream catchment basin. To do this we utilized the U.S. Geological Survey (USGS) National Hydrography Dataset Plus (NHDPlus; https://water.usgs.gov/GIS/metadata/usgswrd/XML/streamgagebasins.xml). This database contains the location of 19 031 stream gauges with corresponding catchment basin boundaries.

For each flood event, we searched for a stream gauge located inside the event polygon and computed the mean radar coverage metric over the matching source basin (Fig. 3). If more than one stream gauge was found inside the event polygon, then the radar coverage metric means were computed over all corresponding basins. If no stream gauge was situated in the polygon, then we looked for the nearest stream gauge; if the distance to the mean polygon latitude–longitude coordinate was less than 10 km, the stream gauge match was accepted. (This means the matched stream gauge was even closer to the polygon border.) With this procedure, 24 236 flash flood events were matched to source basins over the analysis period. All the analyses conducted on flash floods described in the rest of this paper were based on this set of events.

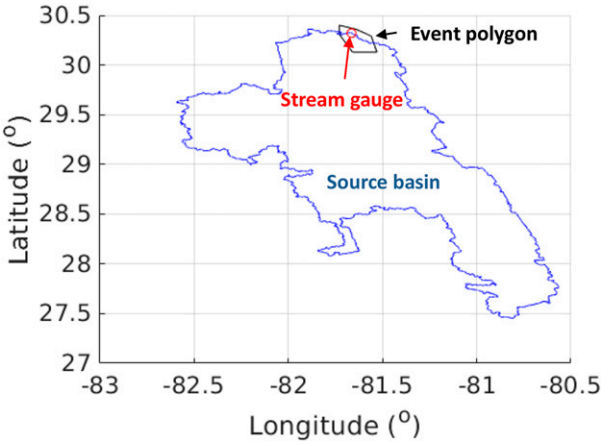

FIG. 3. Illustration of how a flood event is matched to the source basin.

d. *Detection probability dependence on radar coverage*

Flash flood warning POD statistics were computed versus the basin-averaged radar coverage parameters (Fig. 4, top row). For FVO, the data were binned using cumulative distribution percentage intervals of [0, 1], (1, 5], (5, 25], (25, 50], (50, 75], and (75, 100]. For CHR, the data were binned using cumulative distribution percentage intervals of [0, 25], (25, 50], (50, 75], (75, 95], (95, 99], and (99, 100]. The asymmetric interval distributions help to draw out the steep change regimes where data were sparse. Note that the abscissa values plotted do not correspond to the center of the data bins—instead, they are the actual means of the binned FVO or CHR data. The vertical and horizontal error bars denote the 95% confidence intervals along both dimensions (see CK19a,b for further details).

Flash flood POD unambiguously increases with FVO and decreases with CHR. This is a very important result because it connects better radar coverage to flash flood warning performance improvement and allows a continuous functional mapping between the two.

Brought to you by NOAA Central Library | Unauthenticated | Downloaded 01/16/24 09:14 PM UTC

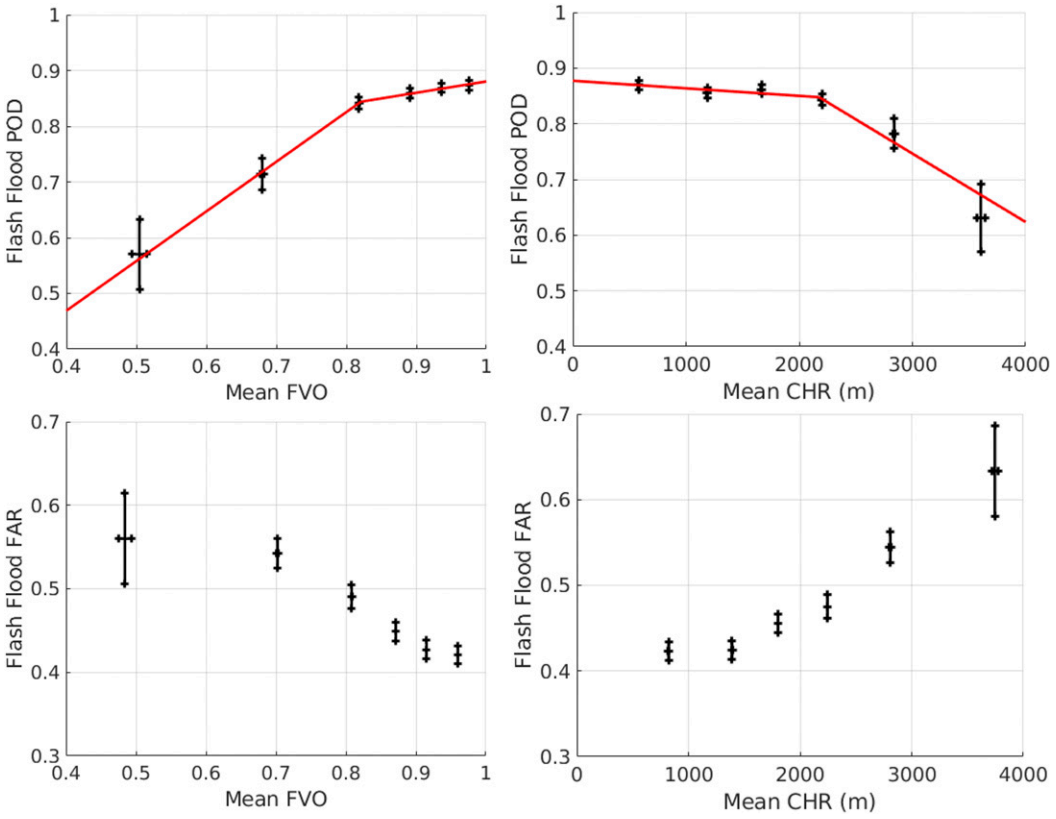

FIG. 4. Plots of (top left) flash flood POD vs FVO, (top right) flash flood POD vs CHR, (bottom left) flash flood FAR vs FVO, and (bottom right) flash flood FAR vs CHR. Solid red lines are linear fits to the data.

(This result is also consistent with a prior study that showed a positive dependence of POD on WSR-88D low-level coverage over NWS WFO areas; Meléndez et al. 2018.) We modeled these relationships by two-segment linear fits with input uncertainty in both dimensions using the "fitexy" function from *Numerical Recipes* (Press et al. 1992). Fitting results are given in Table 1, where a is the y intercept, b is the slope, σ_a and σ_b are the standard deviations of a and b, χ^2 is the fitted chi-squared value, and Q is the goodness-of-fit probability.

As can be seen in the POD-versus-FVO plot of Fig. 4, there is a discernible change in slope between FVO = 0.7 and 0.8. (The slope change is more gradual in the FAR-vs-FVO plot; FAR indicates false alarm ratio) If we assume that all of the observation loss occurs at the bottom of the volume (which is true except for the small fraction attributable to the radar cone of silence at the top of the volume), FVO = (20 kft − minimum observation height)/20 kft. Note, then, that FVO of 0.7 and 0.8 approximately correspond to floors of 6000 and 4000 ft AGL. Thus, if one had to pick one altitude as the "critical floor" for radar coverage with respect to flash flood warning performance, it would be ~5000 ft AGL; the top-left plot in Fig. 2 corresponds to this height.

Flash flood detection can be defined based on only positive lead times or all lead times (including zero and negative lead times). We decided on the latter because the casualty regression statistics were better with all lead times included (section 2h). For a measure of model sensitivity, we also did the analysis with detections defined with only positive lead times. As expected, the primary impact of excluding zero and negative lead times was to reduce the POD values; however, POD still increased with FVO, POD decreased with CHR, and the fits remained significant.

TABLE 1. POD vs radar coverage parameters (FOV and CHR): linear fit results.

	FVO		CHR	
Segment	Low FVO	High FVO	Low CHR	High CHR
a	0.11	0.68	0.88	1.1
b	0.89	0.20	-1.4×10^{-5}	-1.2×10^{-4}
σ_a	0.12	0.074	0.011	0.075
σ_b	0.15	0.084	8.1×10^{-6}	3.2×10^{-5}
χ^2	0.037	0.13	1.2	0.89
Q	0.85	0.94	0.54	0.35

Brought to you by NOAA Central Library | Unauthenticated | Downloaded 01/16/24 09:14 PM UTC

TABLE 2. Mean CONUS flash flood POD and FAR.

Period	1 Oct 2007–31 Dec 2018	1 Oct 2007–7 Mar 2011	16 May 2013–31 Dec 2018
POD (all lead times)	0.853 ± 0.005	0.857 ± 0.008	0.853 ± 0.006
POD (positive lead times only)	0.774 ± 0.005	0.776 ± 0.010	0.775 ± 0.007
No. of points averaged (POD)	24 236	7097	13 408
FAR	0.452 ± 0.005	0.434 ± 0.010	0.453 ± 0.007
No. of points averaged (FAR)	32 438	9729	17 518

We also tried combining the FVO and CHR relationships in the flash flood POD model via weighted additions of the two relationships. The mean-square sums of the difference between data and model were minimized to obtain the optimal weighting. The error was minimized with a 0.86 weight on the FVO relationship and a 0.14 weight on the CHR relationship.

e. False alarm ratio dependence on radar coverage

To compute flash flood warning FAR statistics versus the radar coverage metrics, we matched each warning to the relevant catchment basin(s) following the method outlined in section 2c for flood events. In this case, however, the event polygon depicted in Fig. 3 is replaced by the warning polygon. With this procedure, 32 438 flash flood warnings were matched to source basins over the analysis period. (All of the analyses conducted on flash floods described in the rest of this paper were based on this set of warnings.) The radar coverage parameter values were then averaged over the corresponding basin boundaries.

The resulting plots of FAR versus basin-averaged radar coverage parameters are shown in the bottom row of Fig. 4. For FVO, the data were binned using cumulative distribution percentage intervals of [0, 1], (1, 10], (10, 25], (25, 50], (50, 75], and (75, 100]. For CHR, the data were binned using cumulative distribution percentage intervals of [0, 25], (25, 50], (50, 75], (75, 90], (90, 99], and (99, 100].

FAR clearly decreases with FVO and increases with CHR. This result is consistent with an earlier analysis that showed a negative dependence of FAR on WSR-88D low-level coverage over NWS WFO areas (Meléndez et al. 2018). Unfortunately, however, because the casualty regression analysis did not yield a statistically meaningful relationship between historical FAR and casualty rate (section 2h), we were not able to exploit this clear dependency of flash flood FAR on radar coverage for our benefit model. (Hence, linear fits to the bottom-row plots in Fig. 4 are not given.)

Note that we did not use a combined warning performance metric such as the critical success index (CSI) for a couple of reasons. First, POD could be applied to the casualty regression model (section 2h) on a per-event basis via the binary warning presence variable, whereas FAR and CSI could not. Second, for a geospatial mapping of historical warning performance (for use by the regression model), the mismatch in spatial boundaries for computing POD (event polygons) and FAR (warning polygons) presented a problem in combining them for CSI; hence, only FAR was tried for that purpose.

As for warning lead time, our analysis did show a positive correlation between increased radar coverage and lead time. However, because flash flood lead time did not correlate negatively with casualty rate (section 2h), we could not include it as part of our benefit model.

f. Impact of dual-polarization upgrade

To investigate the impact of the WSR-88D dual-polarization upgrade on flash flood warning performance, we computed the mean CONUS POD and FAR over two periods: 1) from 1 October 2007 to 7 March 2011 and 2) from 16 May 2013 to 31 December 2018. As explained in section 2b, these dates were chosen based on the first operational CONUS dual-polarization deployment (8 March 2011) and the completion of the CONUS upgrade deployment (16 May 2013). Table 2 lists the corresponding POD and FAR values for these periods as well as for the entire analysis period. The plus/minus values indicate the 95% confidence intervals for the means.

The mean flash flood warning values did not yield statistically meaningful differences between the single-polarization and dual-polarization eras. This stands in contrast to case studies that showed dramatic improvement in flash flood warning performance when the nation's meteorological radar network was upgraded to the WSR-88D from the WSR-57 and WSR-74 (Polger et al. 1994). One of the challenges with QPE in the dual-polarization era is the ongoing difficulty with calibration of differential reflectivity Z_{DR}, leading to difficulties obtaining consistent QPE results for use in the flash flood warning process (Ryzhkov et al. 2005). As a result, the NWS has approved the transition to the "rainfall accumulation method using specific attenuation" [$R(A)$] algorithm (Snow 2017). The $R(A)$ technique uses a slope

Brought to you by NOAA Central Library | Unauthenticated | Downloaded 01/16/24 09:14 PM UTC

of the Z_{DR}/Z (horizontal reflectivity factor), meaning that constant offsets in Z_{DR} across the tilt/volume theoretically will not cause as much of an error in QPE (Cocks et al. 2018; Ryzhkov and Zrnić 2019). Initial results of the $R(A)$ algorithm have shown promise relative to the $R(Z, Z_{DR})$ method when polarimetric bias is introduced (Kurdzo et al. 2019, manuscript submitted to *J. Appl. Meteor. Climatol.*). It is possible that the eventual use of $R(A)$ will impact our results in the future.

The good news is that the statistics of flash flood warning versus radar coverage as exemplified by the Fig. 4 plots were very stable over the single- and dual-polarization periods. This was another confirmation that these relationships are meaningful and robust, and it further justified their use in the benefit estimation model.

g. *Non–flash flood warnings versus radar coverage*

Although this study focused on flash floods (and they account for the majority of flood-related fatalities; Ashley and Ashley 2008), we took the opportunity to investigate the relationship between radar coverage and non–flash flood warning performance. Using the same procedure employed for the flash flood analysis yielded no discernible coherent relationship between POD and FVO or CHR, and between FAR and FVO or CHR. These null results are perhaps not surprising, given that warning decisions for longer-term events must be based primarily on model forecast data, and the importance of QPE to the flood forecasting process diminishes with increasing time horizon as stream gauge data and quantitative precipitation forecast (QPF) become more relevant (e.g., Hudlow et al. 1984). These results preclude the addition of non–flash floods to our radar network benefit model.

h. *Casualty dependence on flash flood warning*

With the causal link between radar coverage and flash flood warning performance clearly established, we proceed to discuss the connection between flash flood warnings and casualty rates. Among the factors that are thought to affect flash flood casualty rate are population, time of day, building type, catchment basin size, water flow velocity and depth, rate of water-level rise, and warning lead time, and they appear to interact in various ways to impact casualty rates. For example, while most casualty events occur around headwater catchments in rural areas (because flash floods are generated by the rapid response time of small basins to heavy rainfall), when they do occur downstream in urban areas, the casualty rates are higher (Špitalar et al. 2014). The same article reports that while flash flood occurrence in the United States peaks around 1700 local time (LT), the per-event casualty rate reaches a maximum at 2100 LT, hinting at the importance of human factors such as inability to see in the dark for those outside. We refer the reader to informative past reviews on this topic (e.g., Jonkman et al. 2008; Smith and Rahman 2016). For the purposes of developing a radar network benefit model, only variables that could be geospatially characterized were considered. Temporal predictors like season and time of day were excluded, since they were not germane to our time-independent benefit model. However, in the future, the model could be extended to capture temporal effects.

The flash flood casualty variance was more than 20 times as large as the mean statistics over our analysis period. Thus, instead of a Poisson distribution that is often used for counting statistics, we adopted a negative binomial distribution model for the casualty count,

$$C \sim \text{NegBin}(\mu, \theta), \tag{1}$$

for our casualty regression analysis, where μ is the distribution mean and θ is the dispersion parameter. The regression model then was a linear combination of candidate predictor variables set equal to $\ln\mu$ This is the same scheme that we used for the CK19a,b tornado study.

At this point, casualties were not divided between fatalities and injuries. Since the vast number of events have zero (no casualty) outcomes, increasing the number of nonzero outcome cases by aggregating fatalities and injuries improves statistical robustness. While the database includes direct and indirect casualties separately, we only used direct casualties in our analysis because we sought the tightest causal bond between flash floods and their effects on people. In the monetization stage (section 2i), we parsed the model results into fatalities and two types of injuries on the basis of historical averages.

The predictor variables that we tried in the regression analysis were 1) logarithm of the population, 2) fraction of population in mobile housing, 3) historical flash flood warning FAR, 4) catchment basin size (as a proxy for basin response time), 5) flood ''flashiness,'' 6) flash flood warning presence (binary—0 or 1), and 7) flash flood warning lead time. Variables 1, 2, and 3 were averaged over the flood event polygon. The predictor variables were tested both individually and in combination to elucidate any cross-correlation effects. We also tried FVO and CHR (averaged over the source basins) as casualty predictors to see if a direct link could be established between radar coverage and casualty rate, but there was no meaningful statistical relationship, consistent with the findings of Meléndez et al. (2018).

We acquired population data from the Center for International Earth Science Information Network

Brought to you by NOAA Central Library | Unauthenticated | Downloaded 01/16/24 09:14 PM UTC

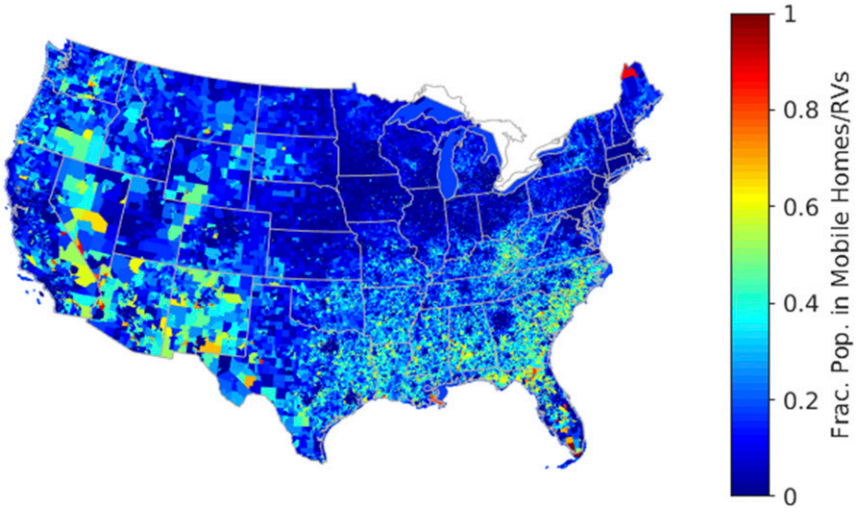

FIG. 5. Fraction of population living in mobile housing as derived from the 2015 American Community Survey data given at the census block group level.

(CIESIN 2017) with latitude–longitude spacing that matched our 30-arc-s model grid resolution. Measured population for 2005, 2010, and 2015 were available, as well as projected population for 2020; linear interpolation yielded corresponding data for the other years. In a nod to statistics that showed most flash flood fatalities occurring while people were away from their residences (predominantly while driving, but also during hiking, camping, etc.; Terti et al. 2017), we set a floor of 1 in the population field everywhere. Also, in cases where the event casualty count exceeded the population in the event polygon, the population was set to the casualty count for logical consistency. Otherwise, we relied on a general spatial correlation between residential population and transient mobile population.

Flood flashiness, defined as the peak flow above flood stage divided by the product of basin area and time from flood stage exceedance to peak flow (Saharia et al. 2017), was considered because it seemed to hold promise as a predictor of flash flood casualty rate. Since the NWS storm events database did not contain quantitative data on water flow or depth, we computed flashiness from USGS streamflow measurements (2016V1; https://blog.nssl.noaa.gov/flash/database/database-2016v1/) archived under the FLASH database (Gourley et al. 2013). However, in comparing the NWS flash flood events with the USGS streamflow measurements by time and location, only a small fraction of the former were found to match with the latter. Therefore, any casualty regression results that included flashiness as a predictor variable were handicapped by the reduction in input data points.

The fraction of the population living in mobile housing was an effective predictor variable for tornado casualties (CK19a,b). Intuitively, one might expect the heightened vulnerability of mobile housing to be washed away by flood waters to be a factor in casualty rate. In fact, about a third of building-related flash flood casualties was estimated to have occurred in mobile homes (Terti et al. 2017). Mobile housing and trailer parks are also often located near rivers (Marrero 1979), while a proposed flash flood severity index codifies the sweeping away of mobile homes as a category-defining characteristic (Schroeder et al. 2016). The gridded fraction of the population in mobile housing were computed from data obtained from the American Community Survey database for 2015 (U.S. Census Bureau 2016) and the Decennial Census for 2000 (Manson et al. 2018). We combined the population in the ''mobile home'' and ''boat, RV, van, etc.'' categories to arrive at the mobile housing population, which was normalized by the total population in each census block group to yield the fraction of population in mobile housing. We sampled and mapped this data to our 30-arc-s latitude–longitude model grid. See CK19a,b for further details. In the regression analysis, linearly interpolated maps (between 2000 and 2015) were used for 2007–14, and the 2015 map (Fig. 5) was used for 2015–18.

For the negative binomial regression analysis, we utilized the ''glm.nb'' function from the open software package R (https://www.R-project.org/). An exhaustive search of predictor combinations yielded a clear winner that was based on statistical reliability. The best regression fit statistics were obtained by keeping only population P, fraction of population in mobile housing M, and warning presence W in the statistical model,

Brought to you by NOAA Central Library | Unauthenticated | Downloaded 01/16/24 09:14 PM UTC

TABLE 3. Flash flood casualty model regression results.

Parameter	Estimate	Std error	z	Pr (>|z|)
α	0.166	0.020	8.13	4×10^{-16}
β	2.20	0.435	5.05	4×10^{-7}
γ	−0.572	0.160	−3.59	3×10^{-4}
k	−4.58	0.206	−22.2	$<2 \times 10^{-16}$
θ	0.105	7.16×10^{-4}	—	—

$$\ln\mu = \alpha \ln P + \beta M + \gamma W + k, \tag{2}$$

where k is the intercept constant and α, β, and γ are the regression coefficients. For the definition of warning presence, we tried including all lead times versus only positive lead times, and the better result was obtained by including all lead times. The fit results are given in Table 3. The probability of the "null hypothesis being true" for each predictor was less than 0.0003, which is much smaller than the typically used threshold of 0.05. In addition, comparison of the casualty regression relation with and without each predictor via degree-of-freedom chi-squared tests showed that each variable was a statistically significant predictor.

Applying the same flash flood events input data to Eq. (2) with the estimated coefficients gave a casualty count of 681, which is reasonably close to the actual count of 631. The presence of a flash flood warning reduces casualty rate by 44% according to this model.

i. Monetizing casualties

The value of a statistical life (VSL) is commonly used to monetize casualties in benefit analyses. As we did previously (CK19a,b), we followed the guidance of the U.S. Department of Transportation (DOT; Moran and Monje 2016), which established a VSL of $9.6 million (M) in 2015 dollars. To update the value to 2019 dollars, we used the DOT's equation,

$$\mathrm{VSL}_T = \mathrm{VSL}_0 \frac{\mathrm{CPI}_T}{\mathrm{CPI}_0} \left(\frac{\mathrm{MUWE}_T}{\mathrm{MUWE}_0}\right)^q, \tag{3}$$

where CPI is the consumer price index, MUWE is the median usual weekly earnings, q is income elasticity, and the subscripts T and 0 signify updated base year and original base year. We got $\mathrm{CPI}_T/\mathrm{CPI}_0 = 1.08$ (https://www.bls.gov/data/inflation_calculator.htm) and $\mathrm{MUWE}_T/\mathrm{MUWE}_0 = 1.12$ (https://www.bls.gov/cps/cpswktabs.htm) from the U.S. Bureau of Labor Statistics database, for a baseline of January 2015 and updated time of January 2019. Taking the DOT's recommended value of $q = 1$ yielded a 2019 VSL of $11.6 M.

We did not distinguish between fatalities and injuries in our casualty regression model as explained in section 2h. We used the actual mean ratio calculated over the analysis period to parse the model output into the two casualty types, which yielded 61% fatalities and 39% injuries.

Injuries were monetized as fractions of VSL, relying on a Federal Emergency Management Administration (FEMA) formulation (FEMA 2009) specifying injuries requiring hospitalization as level 4 and injuries resulting in treatment and release as level 2. With the DOT setting level-4 injury cost at 0.266 × VSL and level-2 injury cost at 0.047 × VSL (Moran and Monje 2016), these costs are $3.09M and $0.545M, respectively, in 2019 dollars.

Because the flood event database does not categorize injuries by severity, we scoured the internet for papers and news reports that contained flash flood injury outcome information. We found usable reports on 12 events between 1956 and 2018 with 3336 total injuries, with the count being dominated by the 9 June 1972 Rapid City, South Dakota, event. To avoid being biased by one event, we computed the ratio of injury types for each event and then took the mean of the ratios. The result was 43% for injuries requiring hospitalization versus 57% for injuries that were treated and released.

j. CONUS grid computation

All of the individual model components can now be integrated to generate mean annual CONUS flash flood casualty cost. The modeled casualty rate (per year, per grid cell) is given by

$$R_{ij}^{F,H,R} = Y^{F,H,R}[r_{ij}(1)B_{ij} + r_{ij}(0)(1 - B_{ij})]O_{ij}, \tag{4}$$

where B is the probability of warning per flash flood (POD), O is the flash flood occurrence rate, i and j are the latitude and longitude grid indices, and the superscripts indicate fatal (F), injured—hospitalized (H), and injured—treated and released (R). The gridcell size is 1/120° × 1/120°. The casualty-type fractions are broken down as

$$Y^F = f, \tag{5}$$

$$Y^H = (1 - f)h, \quad \text{and} \tag{6}$$

$$Y^R = (1 - f)(1 - h), \tag{7}$$

where f is the fatality fraction and h is the fraction of injured that are hospitalized. From Eq. (2) we get the casualty rate per flash flood,

$$r_{ij}(W) = \exp[\alpha \ln(P_{ij}) + \beta M_{ij} + \gamma W + k], \tag{8}$$

with ($W = 1$) and without ($W = 0$) a flash flood warning.

To generate the flash flood POD map, we applied the Table 1 fitted parameters to the radar network FVO and

Brought to you by NOAA Central Library | Unauthenticated | Downloaded 01/16/24 09:14 PM UTC

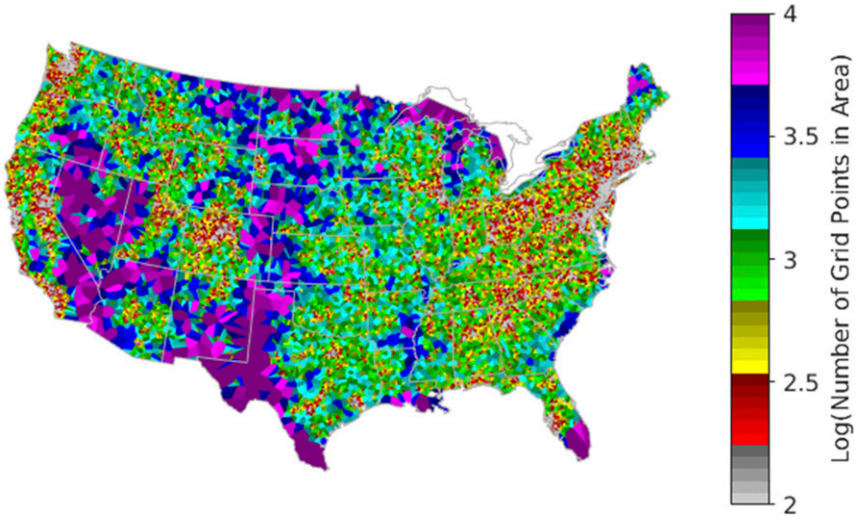

FIG. 6. Areas associated with nearest USGS NHDPlus stream gauge colored according to the logarithm of the number of grid points enclosed.

CHR maps and summed them with weights given in section 2d. However, a geospatial mapping was needed because Eq. (4) is computed over the grid cells of flash flood occurrence, not radar observation of the source rainfall. Thus, we mapped every CONUS grid cell to the nearest USGS NHDPlus stream gauge (Fig. 6), which was mapped to the corresponding source basin grid cells. The modeled flash flood POD computed based on mean radar FVO and CHR over the source basins were then able to be mapped onto the flash flood occurrence areas. The modeled POD values were computed from $0.86 \times \text{POD(FVO)} + 0.14 \times \text{POD(CHR)}$. POD(FVO) and POD(CHR) were calculated using the piecewise-linear relationships given by the a (y intercept) and b (slope) coefficients in Table 1 (and expressed by the red lines in Fig. 4). The resulting flash flood POD map for the current WSR-88D network is shown in Fig. 7.

The mean annual flash flood occurrence rate was computed for each CONUS grid cell using the NWS storm database over the period 2006–18. Earlier NWS data were not used because the cause of flooding was not recorded. To obtain better coverage and statistics (since flash floods occur relatively rarely and the NWS database is not a comprehensive source), we also computed occurrence rate with the USGS streamflow measurements that date back to 1936, based on exceedance of the action stage. Since these observations came from single point locations, we counted the floods as having occurred in the four closest grid cells. In joining the results from the two disparate datasets, we took the greater

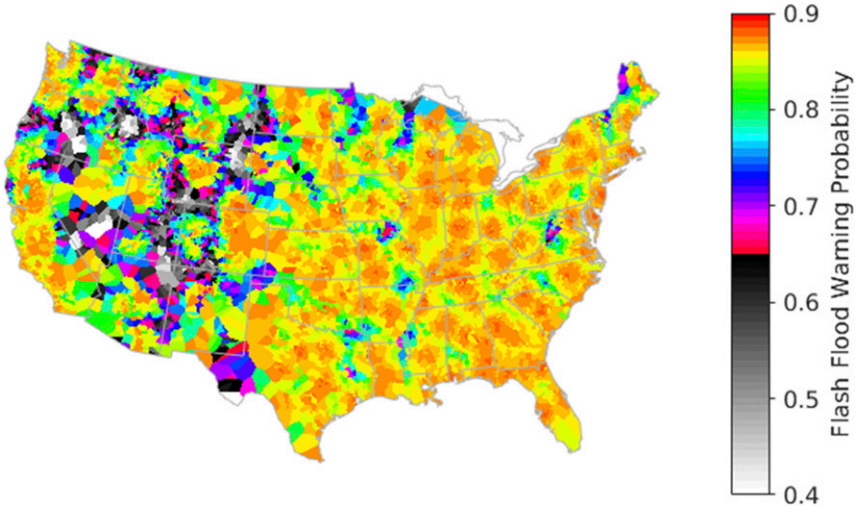

FIG. 7. Modeled flash flood warning probability for the current WSR-88D network.

Brought to you by NOAA Central Library | Unauthenticated | Downloaded 01/16/24 09:14 PM UTC

FIG. 8. Mean annual flash flood occurrence rate density with the rates mapped from the event locations to the corresponding source basins, computed on the basis of combined USGS and NWS flash flood data from 1936 to 2018.

occurrence rate value in each grid cell instead of combining them in order to avoid double counting. For visualization purposes, Fig. 8 shows the mean annual CONUS flash flood occurrence rate density mapped from the event locations to the corresponding source basins. Without this mapping, the occurrence rates at the actual locations are too small to be discernible at the national level—they appear as sparse dots on the CONUS map.

We arrived at the predicted CONUS flash flood casualty rate parsed by casualty type by summing Eq. (4) over all grid indices. The total estimated annual CONUS flash flood casualty cost was obtained by multiplying the individual casualty rates with the corresponding casualty type costs and summing.

3. Example results

To estimate the value provided by the current radar network, as well as the remaining benefit pool, we computed modeled flash flood casualty costs for three basic scenarios: the current WSR-88D network, no radar coverage, and perfect WSR-88D-like coverage. No radar coverage was simulated by setting FVO = 0 and CHR = ∞ everywhere. Perfect WSR-88D-like coverage was simulated by setting FVO = 1 and CHR = 0 everywhere.

Table 4 lists the flash flood casualty estimates for all scenarios and the actual average annual casualty rates. The agreement between the baseline model estimates and the actual casualty rates is very good, especially with the median actual rates. Table 5 gives the corresponding flash flood casualty costs in 2019 dollars.

Differences from the current baseline are provided in the "delta baseline" columns of Tables 4 and 5. This shows that today's WSR-88D network provides over $300M in flash flood benefits annually relative to a CONUS without weather radars. Perfect radar coverage of the CONUS yields a benefit of only $13M yr^{-1} over the baseline. The remaining benefit pool with respect to improved coverage is, therefore, very modest for flash

TABLE 4. Annual CONUS flash flood casualty estimates. Actual average injured counts are totals and are not broken out by injury type.

Scenario	Fatal	Injured (hospitalized)	Injured (treated and released)	Total	Delta baseline
WSR-88D	52.6	14.5	19.2	86.3	—
No radar coverage	77.6	21.4	28.4	127.4	41.1
Perfect coverage	51.5	14.2	18.9	84.6	−1.7
0% warned	83.6	23.1	30.6	137.2	50.9
100% warned	47.2	13.0	17.3	77.4	−8.9
Actual mean (2007–18)	63 ± 10		41 ± 15	104 ± 20	—
Actual median (2007–18)	59 ± 7		23 ± 8	86 ± 13	—

Brought to you by NOAA Central Library | Unauthenticated | Downloaded 01/16/24 09:14 PM UTC

TABLE 5. Annual CONUS flash flood casualty cost estimates.

Scenario	Fatal ($M)	Injured (hospitalized) ($M)	Injured (treated and released) ($M)	Total ($M)	Delta baseline ($M)
WSR-88D	609.9	44.8	10.5	665.2	—
No radar coverage	899.8	66.1	15.5	981.3	316.1
Perfect coverage	597.7	43.9	10.3	651.9	−13.3
0% warned	969.6	71.2	16.7	1057.4	392.2
100% warned	547.0	40.2	9.4	596.5	−68.7

flood casualty reduction, especially when compared with the tornado case, which has an order-of-magnitude larger benefit pool (CK19a). Evidently, for the purposes of QPE to support flash flood warning decisions, the coverage provided by the current baseline is very good.

To estimate the benefit provided by flash flood warnings independent of radar coverage, we also ran the model on a CONUS with no flash flood warnings and with 100% warnings (Tables 4 and 5). The results indicate that over \$390M yr^{-1} benefit is realized by the current flash flood warning system compared to a world without warnings, and the remaining benefit pool for warnings is about \$69M yr^{-1}—this corresponds to the hypothetical situation of having 100% warning on flash floods. (The impact of lead time and false alarm ratio improvements could not be modeled because these variables were not statistically significant predictors of casualty rate.) This value also corresponds to the upper-bound benefit for radars, since, in principle, improvements to radar QPE through noncoverage aspects such as rapid scanning and product algorithm enhancements could help push flash flood POD toward 100%.

Because the average fraction of injured that are hospitalized ($h = 0.43$) used in the model was based on a small number of cases, we tested the model sensitivity by changing this parameter to 0.25 and 0.75. For $h = 0.25$, the magnitude of the benefits in Tables 4 and 5 decreased by 2%, and for $h = 0.75$, the magnitude of the benefits increased by 4%. Thus, the model appears to be fairly stable with respect to even large variances in this parameter.

Figure 9 shows geospatially the casualty cost density difference between perfect radar coverage and the WSR-88D network. The cost densities were mapped from the casualty locations to the source basins of the flash floods in order to show where improvements in radar coverage may help with respect to flash flood casualty reduction. Impacts from both the flash flood occurrence rate (Fig. 8) and modeled warning probability (Fig. 7) are discernible in Fig. 9. For example, the mountainous region west of Charlottesville, Virginia, has both fairly high flash flood occurrence rate and low modeled warning probability (corresponding to a radar coverage gap noticeable in the Fig. 2, 5000-ft AGL plot), resulting in a larger benefit pool. The poor low-altitude radar coverage in the mountain west, however, does not generally lead to a greater benefit pool, except in areas with more frequent occurrence of flash floods (and perhaps population).

FIG. 9. Modeled annual flash flood casualty cost density difference between the current WSR-88D network and perfect WSR-88D-like coverage.

Brought to you by NOAA Central Library | Unauthenticated | Downloaded 01/16/24 09:14 PM UTC

There are, of course, a number of cautionary notes regarding this analysis. First is the incomplete nature of the flash flood data. For example, the NWS flood event data are based on reports by human observers, and floods that occurred in remote locations or had no impact on people may have been missed. Fortunately, the benefits are accumulated in areas with people, so biases in the event data may not greatly affect the modeled benefit estimates. Rapid housing development in remote areas prone to flooding, however, might lead to slight localized underestimates of future benefits.

Second, there are factors that influence the flash flood warning decision process not accounted for in our model, such as the skill of individual forecasters, procedural heterogeneity across regional forecast centers, evolution of the QPE and FFG products, FFG errors, density of rain gauge network, availability of other data sources, storm type, and basin hydrological features. Also, temporal evolution of a basin, such as when a fire decimates vegetation, can greatly affect runoff response time. However, as the statistical stability of the radar-coverage-to-warning-performance relationship over the pre- and post-dual-polarization eras attests, variances due to these other factors appear to largely get averaged out over the large number of data points ingested in the analysis.

The circumstances of flash flood casualties are very complex and difficult to model statistically. Many flash flood fatalities in the United States occur while the victims are away from their residences, which cannot be precisely characterized with population data. It is difficult to capture factors like real-time access to flash flood warnings and likelihood of response (Knocke and Kolivras 2007; Parker et al. 2009; Morss et al. 2016), while data on event characteristics such as flow speed and depth are not universally available. In our casualty regression analysis, we considered potential causative factors with data available geospatially on a national basis and discarded those that were not statistically reliable predictors. The resulting regression model is necessarily a simple one, but, again, the large number of data points used in the analysis provides a high level of statistical robustness that would not be available in a more detailed case study.

4. Summary discussion

We constructed a geospatial model for computing meteorological radar network benefits for flash flood casualty reduction. We showed unambiguously that better radar coverage of the causative rainfall leads to improved flash flood warning statistics. We also established that the casualty rate decreases by 44% when a flash flood warning is present. Combining these two effects, the model was able to generate benefit estimates on a high-resolution spatial grid. The model can work on an arbitrary radar network configuration.

Our model showed that today's WSR-88D network provides over \$300M yr^{-1} in flash flood casualty reduction. There is a modest remaining benefit pool of \$13M yr^{-1} for coverage improvements, which is indicative of the effective coverage provided for this purpose by the current weather radar network. Inclusive of all aspects of flash flood warning POD improvements, including better radar QPE, the maximum benefit pool is \$69M yr^{-1}.

A radar benefit model could not be established for non–flash floods, since our analysis did not yield a meaningful relationship between radar coverage and warning performance. This negative result was not entirely a surprise, given that warning decisions for longer-term events must be based primarily on model forecast data, and the importance of QPE to the flood forecasting process diminishes with increasing time horizon as stream gauge data and QPF become more relevant.

Potential benefits from flash flood property damage reduction could be worth investigating, although loss mitigation options may be limited in this scenario (relocating vehicles, moving valuables from basements and first floors to upper levels, etc.). Also, damage reduction is expected to be less for shorter-lead-time flash flood events relative to longer-lead-time non–flash flood events (Day 1970). A preliminary analysis using population as a proxy for property value did not yield any statistically meaningful relationship between flash flood warning performance and property damage. For a proper study, geospatial data of real estate property type and value as well as vehicle count would likely be needed.

Acknowledgments. We sincerely thank the following people: Chris Miller for acquiring and processing the housing-type data; Angie Locknar for gathering news reports of flash flood injury type statistics; J. J. Gourley, Pierre Kirstetter, and Berry Wen for providing valuable technical guidance; and Kurt Hondl and Mark Weber for supporting this project. This paper has been approved for public release: distribution is unlimited. This material is based upon work supported by the National Oceanic and Atmospheric Administration under Air Force Contract FA8702-15-D-0001. Any opinions, findings, conclusions, or recommendations expressed in this material are those of the authors and do not necessarily reflect the views of the National Oceanic and Atmospheric Administration.

Brought to you by NOAA Central Library | Unauthenticated | Downloaded 01/16/24 09:14 PM UTC

REFERENCES

Ahnert, P., E. Clark, P. Corrigan, and H. White, 2012: National Weather Service flash flood warning services. *26th Conf. on Hydrology*, New Orleans, LA, Amer. Meteor. Soc., TJ7.2, https://ams.confex.com/ams/92Annual/webprogram/Manuscript/Paper199494/marfc_ahnert_ams_final.pdf.

Ashley, S. T., and W. S. Ashley, 2008: Flood fatalities in the United States. *J. Appl. Meteor. Climatol.*, **47**, 805–818, https://doi.org/10.1175/2007JAMC1611.1.

Austin, P. M., and A. C. Bemis, 1950: A quantitative study of the ''bright band'' in radar precipitation echoes. *J. Meteor.*, **7**, 145–151, https://doi.org/10.1175/1520-0469(1950)007<0145:AQSOTB>2.0.CO;2.

Balakrishnan, N., and D. S. Zrnić, 1990: Estimation of rain and hail rates in mixed-phase precipitation. *J. Atmos. Sci.*, **47**, 565–583, https://doi.org/10.1175/1520-0469(1990)047<0565:EORAHR>2.0.CO;2.

Cecinati, F., M. A. Rico-Ramirez, G. B. M. Heuvelink, and D. Han, 2017: Representing radar rainfall uncertainty with ensembles based on a time-variant geostatistical error modelling approach. *J. Hydrol.*, **548**, 391–405, https://doi.org/10.1016/j.jhydrol.2017.02.053.

Chandrasekar, V., H. Chen, and M. Maki, 2012: Urban flash flood applications of high-resolution rainfall estimation by X-band dual-polarization radar network. *Proc. SPIE*, **8523**, 85230K, https://doi.org/10.1117/12.977602.

Cho, J. Y. N., 2015: Revised Multifunction Phased Array Radar (MPAR) network siting analysis. MIT Lincoln Laboratory Project Rep. ATC-425, 84 pp., https://www.ll.mit.edu/sites/default/files/publication/doc/2018-05/Cho_2015_ATC-425.pdf.

——, and J. M. Kurdzo, 2019a: Monetized weather radar network benefits for tornado cost reduction. MIT Lincoln Laboratory Project Rep. NOAA-35, 88 pp., https://www.ll.mit.edu/sites/default/files/publication/doc/monetized-weather-radar-network-benefits-cho-noaa-35.pdf.

——, and ——, 2019b: Weather radar network benefit model for tornadoes. *J. Appl. Meteor. Climatol.*, **58**, 971–987, https://doi.org/10.1175/JAMC-D-18-0205.1.

CIESIN, 2017: Gridded population of the world, version 4 (GPWv4): Population density, rev. 10. NASA Socioeconomic Data and Applications Center, Center for International Earth Science Information Network, accessed 11 December 2017, https://doi.org/10.7927/H4DZ068D.

Clark, R. A., J. J. Gourley, Z. L. Flamig, Y. Hong, and E. Clark, 2014: CONUS-wide evaluation of National Weather Service flash flood guidance products. *Wea. Forecasting*, **29**, 377–392, https://doi.org/10.1175/WAF-D-12-00124.1.

Cocks, S. B., L. Tang, Y. Wang, J. Zhang, A. Ryzhkov, P. Zhang, and K. W. Howard, 2018: MRMS precipitation estimates using specific attenuation. *32nd Conf. on Hydrology*, Austin, TX, Amer. Meteor. Soc., 77, https://ams.confex.com/ams/98Annual/webprogram/Paper335167.html.

Day, H. J., 1970: Flood warning benefit evaluation—Susquehanna River basin (urban residences). ESSA Tech. Memo. WBTM HYDRO 10, 42 pp.

DeKay, M. L., and D. H. McClelland, 1993: Predicting loss of life in cases of dam failure and flash flood. *Risk Anal.*, **13**, 193–205, https://doi.org/10.1111/j.1539-6924.1993.tb01069.x.

FEMA, 2009: FEMA benefit–cost analysis reengineering (BCAR), version 4.5; Tornado safe room module methodology report. Department of Homeland Security Rep., 75 pp., https://www.fema.gov/media-library-data/20130726-1738-25045-0690/tornadomethodology.pdf.

Gourley, J. J., and Coauthors, 2013: A unified flash flood database over the US. *Bull. Amer. Meteor. Soc.*, **94**, 799–805, https://doi.org/10.1175/BAMS-D-12-00198.1.

——, Z. L. Flamig, Y. Hong, and K. W. Howard, 2014: Evaluation of past, present and future tools for radar-based flash-flood prediction in the USA. *Hydrol. Sci. J.*, **59**, 1377–1389, https://doi.org/10.1080/02626667.2014.919391.

——, and Coauthors, 2017: The FLASH project: Improving the tools for flash flood monitoring and prediction across the United States. *Bull. Amer. Meteor. Soc.*, **98**, 361–372, https://doi.org/10.1175/BAMS-D-15-00247.1.

Hudlow, M. D., R. K. Farnsworth, and P. R. Ahnert, 1984: NEXRAD technical requirements for precipitation estimation and accompanying economic benefits. NWS Office of Hydrology Hydro Tech. Note 4, 49 pp.

Jonkman, S. N., J. K. Vrijling, and A. C. W. M. Vrouwenvelder, 2008: Methods for the estimation of loss of life due to floods: A literature review and a proposal for a new method. *Nat. Hazards*, **46**, 353–389, https://doi.org/10.1007/s11069-008-9227-5.

Kirstetter, P., H. Andrieu, G. Delrieu, and B. Boudevillain, 2010: Identification of vertical profiles of reflectivity for correction of volumetric radar data using rainfall classification. *J. Appl. Meteor. Climatol.*, **49**, 2167–2180, https://doi.org/10.1175/2010JAMC2369.1.

Kitzmiller, D., D. Miller, R. Fulton, and F. Ding, 2013: Radar and multisensor precipitation estimation techniques in National Weather Service hydrologic operations. *J. Hydrol. Eng.*, **18**, 133–142, https://doi.org/10.1061/(ASCE)HE.1943-5584.0000523.

Knocke, E. T., and K. N. Kolivras, 2007: Flash flood awareness in southwest Virginia. *Risk Anal.*, **27**, 155–169, https://doi.org/10.1111/j.1539-6924.2006.00866.x.

Kurdzo, J. M., E. F. Clemons, J. Y. N. Cho, P. L. Heinselman, and N. Yussouf, 2018: Quantification of QPE performance based on SENSR network design possibilities. *Proc. 2018 IEEE Radar Conf.*, Oklahoma City, OK, Institute of Electrical and Electronics Engineers, 169–174, https://doi.org/10.1109/RADAR.2018.8378551.

Manson, S., J. Schroeder, D. Van Riper, and S. Ruggles, 2018: IPUMS National Historical Geographic Information System, version 13.0. University of Minnesota, accessed 11 June 2018, https://doi.org/10.18128/D050.V13.0.

Marrero, J., 1979: Danger: Flash floods. *Weatherwise*, **32**, 34–37, https://doi.org/10.1080/00431672.1979.9930069.

McLaughlin, D., and Coauthors, 2009: Short-wavelength technology and the potential for distributed networks of small radar systems. *Bull. Amer. Meteor. Soc.*, **90**, 1797–1818, https://doi.org/10.1175/2009BAMS2507.1.

Meléndez, D., K. Abshire, and J. Sokich, 2018: NEXRAD weather radar coverage and National Weather Service warning performance. *2018 Fall Meeting*, Washington, DC, Amer. Geophys. Union, Abstract A11K-2394, https://doi.org/10.1002/essoar.10500135.1.

Moran, M. J., and C. Monje, 2016: Revised departmental guidance 2016: Treatment of the value of preventing fatalities and injuries in preparing economic analyses. Office of the Secretary of Transportation Memo., 13 pp., https://www.transportation.gov/sites/dot.gov/files/docs/2016%20Revised%20Value%20of%20a%20Statistical%20Life%20Guidance.pdf.

Morss, R. E., K. J. Mulder, J. K. Lazo, and J. L. Demuth, 2016: How do people perceive, understand, and anticipate responding to

Brought to you by NOAA Central Library | Unauthenticated | Downloaded 01/16/24 09:14 PM UTC

flash flood risks and warnings? Results from a public survey in Boulder, Colorado, USA. *J. Hydrol.*, **541**, 649–664, https://doi.org/10.1016/j.jhydrol.2015.11.047.

NOAA, 2019: Weather related fatality and injury statistics. NWS Office of Climate, Water, and Weather Services, https://www.weather.gov/hazstat/.

NWS, 2019: Flash flood. National Weather Service glossary. NOAA, https://w1.weather.gov/glossary/index.php?letter=f.

Ostrowski, J., and Coauthors, 2003: Flash flood guidance improvement team: Final report. NWS Office of Hydrologic Development, 47 pp., http://www.nws.noaa.gov/ohd/rfcdev/docs/ffgitreport.pdf.

Parker, D. J., S. J. Priest, and S. M. Tapsell, 2009: Understanding and enhancing the public's behavioural response to flood warning information. *Meteor. Appl.*, **16**, 103–114, https://doi.org/10.1002/met.119.

Polger, P. D., B. S. Goldsmith, R. C. Przywarty, and J. S. Bocchieri, 1994: National Weather Service warning performance based on the WSR-88D. *Bull. Amer. Meteor. Soc.*, **75**, 203–214, https://doi.org/10.1175/1520-0477(1994)075<0203:NWSWPB>2.0.CO;2.

Press, W. H., S. A. Teukolsky, W. T. Vetterling, and B. P. Flannery, 1992: *Numerical Recipes in C: The Art of Scientific Computing*. 2nd ed. Cambridge University Press, 994 pp.

Rogalus, M. J., III, and F. L. Ogden, 2013: Spatial assessment of five years of WSR-88D data over the Mississippi River basin and its estimation bias around rain gauge sites. *J. Hydrol. Eng.*, **18**, 212–218, https://doi.org/10.1061/(ASCE)HE.1943-5584.0000636.

Ryzhkov, A. V., and D. S. Zrnić, 2019*: Radar Polarimetry for Weather Observations*. Springer, 486 pp.

——, S. E. Giangrande, V. M. Melnikov, and T. J. Schuur, 2005: Calibration issues of dual-polarization radar measurements. *J. Atmos. Oceanic Technol.*, **22**, 1138–1155, https://doi.org/10.1175/JTECH1772.1.

——, P. Zhang, H. Reeves, M. Kumjian, T. Tschallener, S. Trömel, and C. Simmer, 2016: Quasi-vertical profiles—A new way to look at polarimetric radar data. *J. Atmos. Oceanic Technol.*, **33**, 551–562, https://doi.org/10.1175/JTECH-D-15-0020.1.

Saharia, M., P.-E. Kirstetter, H. Vergara, J. J. Gourley, Y. Hong, and M. Giroud, 2017: Mapping flash flood severity in the United States. *J. Hydrometeor.*, **18**, 397–411, https://doi.org/10.1175/JHM-D-16-0082.1.

Saunders, M. E., K. D. Ash, and J. M. Collins, 2018: Usefulness of the United States National Weather Service radar display as rated by website users. *Wea. Climate Soc.*, **10**, 673–691, https://doi.org/10.1175/WCAS-D-17-0108.1.

Schroeder, A. J., and Coauthors, 2016: The development of a flash flood severity index. *J. Hydrol.*, **541**, 523–532, https://doi.org/10.1016/j.jhydrol.2016.04.005.

Sene, K., 2013: *Flash Floods: Forecasting and Warning*. Springer, 386 pp.

Smith, G. P., and P. F. Rahman, 2016: Approaches for estimating flood fatalities relevant to floodplain management. University of New South Wales Water Research Laboratory Tech. Rep. 2015/09, 52 pp., https://knowledge.aidr.org.au/media/2333/wrl-approches-for-estimating-flood-fatalities-september-2016.pdf.

Snow, J., 2017: Recommendation of $R(A)$ technique for QPE. NEXRAD Technical Advisory Committee Memo., 1 p., https://www.roc.noaa.gov/WSR88D/PublicDocs/TAC/2017/February2017NEXRADTAC-Specific%20Attenuation%20QPE%20Decision.pdf.

Špitalar, M., J. J. Gourley, C. Lutoff, P.-E. Kirstetter, M. Brilly, and N. Carr, 2014: Analysis of flash flood parameters and human impacts in the US from 2006 to 2012. *J. Hydrol.*, **519**, 863–870, https://doi.org/10.1016/j.jhydrol.2014.07.004.

Steadman, R. M., and R. A. Brown, 2007: Plan for testing the feasibility of site-specific scanning strategies for WSR-88Ds. *23rd Conf. on Interactive Information Processing Systems (IIPS)*, San Antonio, TX, Amer. Meteor. Soc., 5B.3, https://ams.confex.com/ams/pdfpapers/117708.pdf.

Stensrud, D. J., and Coauthors, 2009: Convective-scale warn-on-forecast system: A vision for 2020. *Bull. Amer. Meteor. Soc.*, **90**, 1487–1500, https://doi.org/10.1175/2009BAMS2795.1.

Terti, G., I. Ruin, S. Anquetin, and J. J. Gourley, 2017: A situation-based analysis of flash flood fatalities in the United States. *Bull. Amer. Meteor. Soc.*, **98**, 333–345, https://doi.org/10.1175/BAMS-D-15-00276.1.

Torres, S., and C. Curtis, 2006: Design considerations for improved tornado detection using superresolution data on the NEXRAD network. *Third European Conf. on Radar Meteorology and Hydrology (ERAD)*, Barcelona, Spain, Amer. Meteor. Soc., 5B.10, https://ams.confex.com/ams/pdfpapers/116240.pdf.

U.S. Census Bureau, 2016: Table B25033: Total population in occupied housing units by tenure by units in structure. 2011–2015 American Community Survey 5-Year Estimates, USCB, accessed 11 June 2018, https://censusreporter.org/tables/B25033/.

Weber, M. E., J. Y. N. Cho, J. S. Herd, J. M. Flavin, W. E. Benner, and G. S. Torok, 2007: The next-generation multimission U.S. surveillance radar network. *Bull. Amer. Meteor. Soc.*, **88**, 1739–1751, https://doi.org/10.1175/BAMS-88-11-1739.

——, ——, and H. G. Thomas, 2017: Command and control for multifunction phased array radar. *IEEE Trans. Geosci. Remote Sens.*, **55**, 5899–5912, https://doi.org/10.1109/TGRS.2017.2716935.

Wen, B., T. Schuur, C. Kuster, and H. Vergara, 2018: Advancing flash flooding early warning using a rapid-scan polarimetric radar observations. *Ninth Int. Precipitation Working Group (IPWG) Workshop*, Seoul, South Korea, Coordination Group for Meteorological Satellites, 15.3, http://www.isac.cnr.it/~ipwg/meetings/seoul-2018/Orals/15-3_Wen.pdf.

Zrnić, D. S., and R. J. Doviak, 1976: Effective antenna pattern of scanning radars. *IEEE Trans. Aerosp. Electron. Syst.*, **AES-12**, 551–555, https://doi.org/10.1109/TAES.1976.308254.

——, and Coauthors, 2007: Agile-beam phased array radar for weather observations. *Bull. Amer. Meteor. Soc.*, **88**, 1753–1766, https://doi.org/10.1175/BAMS-88-11-1753.

Brought to you by NOAA Central Library | Unauthenticated | Downloaded 01/16/24 09:14 PM UTC